MADRID
inter.noise 2019
June 16 - 19
NOISE CONTROL FOR A BETTER ENVIRONMENT

A combined optimization of a general aeroengine inlet for noise reduction

Qiu, Sheng [1]
Department of Discipline Engineering, AECC Commercial Aircraft Engine Co., Ltd.
3998 South Lianhua Road, Shanghai ,China.

ABSTRACT

The fan noise can be not only reduced by acoustic liner, but also controlled by the intake geometry. A novel combined shape optimization and liner optimization to duct acoustic problems is developed with many design parameters. Firstly, the gradient Enhanced Kriging (GEK) and adjoint-method approach have been applied together to design the geometry of intake. It employs a Kriging response surface in the parameter space, augmented with gradients obtained from the continuous adjoint equations efficiently. Secondly, the liner optimization is executed within the prescribed design space based on the Multi-Island Genetic Algorithm. The present paper aims at describing the potential of the combined approach for low noise turbofan duct design. The implementation of the aeroacoustic adjoint method is validated by comparing the gradient values with that obtained by finite differences. The performance of GEK is investigated when gradient information is introduced by using adjoint method. In the liner optimization procedure, the Goodrich model is developed for predicting acoustic impedance of liners. The examples presented demonstrate that significant noise reduction is achieved while the aerodynamic performance maintains by selecting the optimal shape and liner impedance, which confirms the effectiveness and efficiency of the new proposed combined shape and liner optimization framework.

Keywords: Tone Noise, Shape optimization, Liner optimization
I-INCE Classification of Subject Number: 37

1. INTRODUCTION

Recently, the fan noise propagates from the nacelle inlets and bypass duct has become dominant noise sources during take-off and approach stage. And the acoustic liners are often used to tackle this problem. Different methods of optimisation have been employed to optimise acoustic liners to reduce noise efficiently and effectively. Rice has pioneered the acoustic liner optimization technique using numerical approaches[1]. Robinson and Watson study checkerboard liner optimization for a rectangular duct[2]. Motsinger et al. use the optimization technique to design an optimized single element liner in a case without mean flow, and optimized single and dual element liners in cases with mean flow[3]. Hamilton and astley use ACTRAN to

[1] qqqiusheng@126.com

optimize a lip liner in the mid frequency range[4]. Lafronza et al. present an optimization procedure based on a response surface model to investigate a uniform and an axially segmented acoustic liner[5]. The fan noise can be not only reduced by acoustic liner, but also reduced by the geometry of duct. A lot of work which pay attention to geometry optimization are reported.A noise prediction and optimization system for turbofan inlet duct designs is developed by Zheng et al. [6].With the integration of an in-house software suite of CFD codes, and a commercial software ACTRAN, into an in-house optimizer, SOFT[7], liner and geometry optimizations of an axi-symmetric intake are performed by Pan et al.[8] Parametric studies on the effect of duct curvature on noise propagation carried out by Sugimoto et al.[9] have already shown that the effect of scattering and reflection caused by a hardwall geometry increases with duct curvature. McAleer et al. examines the acoustic benefits of a highly curved duct that is incorporated into an engine [10].

However, there is a lot of design variables involved in the aeroacoustic shape optimization. The benefit of using GEK is that the accuracy of the prediction with a given number of samples can be improved by incorporating the gradient information into the Kriging models[11]. Moreover, the gradient needed by GEK can be efficiently computed using the adjoint approach[12]. To explore the merits of both adjoint and Kriging method, a combined adjoint and Kriging method is proposed to facilitate the aeroacoustic shape optimization with many variables firstly. Secondly, the liner optimization is carried out based on the optimum intake duct.

The layout of this paper is as follows. In Section 2, the numerical simulation methods are presented. Section 3 gives an overview of optimization design framework based on a GEK and adjoint-based shape optimization method and a Kriging-based liner optimization method and Section 4 presents the computational results using the optimization algorithm. Finally, Section 5 concludes this paper.

2. THE NUMERICAL SIMULATION METHODS

2.1 Governing Equations of Sound Propogation

The sound wave propagation inside the duct and the radiated sound field in the far field are calculated using LEE method inside of the duct and its near field while a FW-H[13] method is applied in the far field. The complex form of the multimode LEE (MMLEE) method are list as[14]:

$$\begin{cases} \dfrac{\partial \rho'}{\partial t}+u_0\dfrac{\partial \rho'}{\partial x}+v_0\dfrac{\partial \rho'}{\partial r}+\rho_0\left(\dfrac{\partial u'}{\partial x}+\dfrac{\partial v'}{\partial r}\right)+\left(\dfrac{\partial u_0}{\partial x}+\dfrac{\partial v_0}{\partial r}+\dfrac{v_0-imw_0}{r}\right)\rho'+\dfrac{\partial \rho_0}{\partial x}u'+\left(\dfrac{\partial \rho_0}{\partial r}+\dfrac{\rho_0}{r}\right)v'-\dfrac{im\rho_0}{r}w'=0 \\ \dfrac{\partial u'}{\partial t}+u_0\dfrac{\partial u'}{\partial x}+v_0\dfrac{\partial u'}{\partial r}+\dfrac{\partial p'}{\rho_0\partial x}-\dfrac{\partial p_0}{\rho_0^2\partial x}\rho'+\left(\dfrac{\partial u_0}{\partial x}-\dfrac{imw_0}{r}\right)u'+\dfrac{\partial u_0}{\partial r}v'=0 \\ \dfrac{\partial v'}{\partial t}+u_0\dfrac{\partial v'}{\partial x}+v_0\dfrac{\partial v'}{\partial r}+\dfrac{\partial p'}{\rho_0\partial r}-\dfrac{\partial p_0}{\rho_0^2\partial r}\rho'+\dfrac{\partial u_0}{\partial r}u'+\left(\dfrac{\partial v_0}{\partial r}-\dfrac{imw_0}{r}\right)v'=0 \\ \dfrac{\partial w'}{\partial t}+u_0\dfrac{\partial w'}{\partial x}+v_0\dfrac{\partial w'}{\partial r}+\dfrac{w_0}{r}v'+\dfrac{v_0-imw_0}{r}w'-\dfrac{im}{r\rho_0}p'=0 \\ \dfrac{\partial p'}{\partial t}+u_0\dfrac{\partial p'}{\partial x}+v_0\dfrac{\partial p'}{\partial r}+\gamma p_0\left(\dfrac{\partial u'}{\partial x}+\dfrac{\partial v'}{\partial r}\right)+\dfrac{\partial p_0}{\partial x}u'+\left(\dfrac{\partial p_0}{\partial r}+\dfrac{\gamma p_0}{r}\right)v'-\dfrac{im\gamma p_0}{r}w'+\left[\gamma\left(\dfrac{\partial u_0}{\partial x}+\dfrac{\partial v_0}{\partial r}\right)+\dfrac{\gamma v_0-imw_0}{r}\right]p'=0 \end{cases} \tag{1}$$

where superscript ($'$) and subscript (0) are perturbation and mean properties respectively. ρ is the density, p is the pressure, u the axial velocity, v the radial velocity, w the azimuthal velocity, x and r are axial and radial coordinates, and θ is the azimuthal angle. $w_t'=\partial w'/\partial t$ .The fluid is modeled as a perfect gas with the

homentropic assumption, $p^{'} = C_0^2 \rho^{'}$, where C_0 is the sound speed. All variables are nondimensionalized using a reference length L^*, a reference speed C_0^*, and a reference density ρ^*. For the numerical examples presented next, these have been taken as 1 m, 340 m/s, and 1.225 kg/m^3.

2.2 The GEK model And Gradient Computation

The estimate value of original Kriging model is expressed as a summation of a trend function and a Gaussian random process. Compared to that, the GEK model need gradient informantion and can be expressed as the work of Selvakumar et al.[15]:

$$\hat{z}(x^*) = \dot{\hat{\lambda}} + \dot{\varphi}^T \dot{\Psi}^{-1} (\dot{z} - \dot{g}\dot{\hat{\lambda}}) \tag{2}$$

and

$$\dot{\Psi} = \begin{Bmatrix} \Psi & \frac{\partial \Psi}{\partial x_1^{(i)}} & \cdots & \frac{\partial \Psi}{\partial x_v^{(i)}} & \cdots & \frac{\partial \Psi}{\partial x_k^{(i)}} \\ \frac{\partial \Psi}{\partial x_1^{(j)}} & \frac{\partial^2 \Psi}{\partial x_1^{(i)} \partial x_1^{(j)}} & \cdots & \frac{\partial^2 \Psi}{\partial x_1^{(i)} \partial x_v^{(j)}} & \cdots & \frac{\partial^2 \Psi}{\partial x_1^{(i)} \partial x_k^{(j)}} \\ \vdots & \vdots & \ddots & \vdots & \cdots & \vdots \\ \frac{\partial \Psi}{\partial x_u^{(j)}} & \frac{\partial^2 \Psi}{\partial x_1^{(j)} \partial x_u^{(i)}} & \cdots & \frac{\partial^2 \Psi}{\partial x_u^{(i)} \partial x_v^{(j)}} & \cdots & \frac{\partial^2 \Psi}{\partial x_u^{(i)} \partial x_k^{(j)}} \\ \vdots & \vdots & \cdots & \vdots & \ddots & \vdots \\ \frac{\partial \Psi}{\partial x_k^{(j)}} & \frac{\partial^2 \Psi}{\partial x_1^{(j)} \partial x_k^{(i)}} & \cdots & \frac{\partial^2 \Psi}{\partial x_v^{(j)} \partial x_k^{(i)}} & \cdots & \frac{\partial^2 \Psi}{\partial x_k^{(i)} \partial x_k^{(j)}} \end{Bmatrix} \tag{3}$$

Where, x^* is prediction point, g is a column vector of ones and $\dot{\Psi}$ is a $(k+1)n \times (k+1)n$ symmetric block matrix, $\dot{\varphi} = \left(\varphi, \ \frac{\partial \varphi}{\partial x_1}, \ \cdots, \ \frac{\partial \varphi}{\partial x_k} \right)^T$ is the correlation vector and k is the dimensionality of prediction points. Both the function values and gradients of the sample data are contained in the vector $\dot{z} = \left(z, \ \frac{\partial z}{\partial x_1}, \ \cdots, \ \frac{\partial z}{\partial x_k} \right)^T$. θ_m are the hyperparameters of the GEK model,which are determined by maximizing the concentrated likelihood function. And $\hat{z}(x^*)$ is the estimate value of Kriging model. The notations $\frac{\partial \Psi}{\partial x_u^{(j)}}$ means the correlation between function data and u^{th} dimension gradients ,And $\frac{\partial^2 \Psi}{\partial x_u^{(i)} \partial x_v^{(j)}}$ denotes correlation between u^{th} dimension gradients and v^{th}

dimension gradients. $\hat{\dot{\lambda}}$ is the constant trend function for GEK, which is calculated as $\hat{\dot{\lambda}} = (\mathrm{g}^T \dot{\boldsymbol{\Psi}}^{-1} \boldsymbol{g})^{-1} \boldsymbol{g}^T \dot{\boldsymbol{\Psi}}^{-1} \dot{\boldsymbol{z}}$.

For this noise reduction problem, the gradient of acoustic objective function I with respect to the design variables b is given as

$$g = \frac{\delta I}{\delta b} = \frac{1}{\delta b} \left\{ \begin{array}{l} -\int_0^{t_f} \int_{CD} \left(\psi_2 \delta(\frac{\eta_x}{J}) + \psi_3 \delta(\frac{\eta_r}{J}) \right) \frac{p'}{\rho_o} d\xi dt \\ -\int_0^{t_f} \int_{L_1} \left\{ \begin{array}{l} \left[(\frac{1}{\rho_0} \rho' + u' u_0) \delta(\frac{\xi_x}{J}) + u' v_0 \delta(\frac{\xi_r}{J}) \right] \left(\psi_2^+ - \psi_2^- \right) \\ + \left[(\frac{1}{\rho_0} \rho' + v' v_0) \delta(\frac{\xi_r}{J}) + v' u_0 \delta(\frac{\xi_x}{J}) \right] \left(\psi_3^+ - \psi_3^- \right) \end{array} \right\} d\eta dt \\ + \int_D \int_{t_0}^{t_f} \left(\left\{ \frac{\partial \boldsymbol{\psi}^T}{\partial \xi} [\delta(\frac{\xi_x}{J}) \boldsymbol{A} + \delta(\frac{\xi_r}{J}) \boldsymbol{B}] + \frac{\partial \boldsymbol{\psi}^T}{\partial \eta} [\delta(\frac{\eta_x}{J}) \boldsymbol{A} + \delta(\frac{\eta_r}{J}) \boldsymbol{B}] \right\} \boldsymbol{w} dt dD \right. \\ + \int_D \int_{t_0}^{t_f} [\boldsymbol{w} \delta(J^{-1})] \frac{\partial \boldsymbol{\psi}^T}{\partial t} dt dD - \int_{t_0}^{t_f} \int_D \boldsymbol{\psi}^T \boldsymbol{w} \delta(\frac{C'}{J}) dD dt \end{array} \right\} \tag{4}$$

Where, the general cost function I is defined as the amplitude of sound from an inlet duct on the wall and integral line. The advantage is that (4) is independent of δw, the gradient of I can be obtained through one sound-field evaluations. The derivation of gradient formula is described in detail in reference [16]. It's omitted here in consideration of the length of an article.

2.2 Time-Domian Impedance Boundary Condition

The Time-Domian Impedance Boundary Condition (TDIBC) developed by Fung and Ju[17] has been adopted in this paper. For the right moving wave perpendicular to the rigid wall with velocity u, we defined an incident wave and a reflection wave in the frequency domain, which are expressed as $\hat{u}^+$ and $\hat{u}^-$ in terms of Z respecively:

$$\hat{u}^- = \hat{u} - \hat{p} = (1 - Z)\hat{u} \tag{5}$$

$$\hat{u}^+ = \hat{u} + \hat{p} = (1 + Z)\hat{u} \tag{6}$$

A reflection coefficient is defined as $\hat{W} = \hat{u}^- / \hat{u}^+$ in the frequency domain, which is a complex function and can get a direct measure of the magnitude of the reflection. It can also show us a phase relation between the incident wave and the reflection wave. In time domain, $\hat{u}^- = \hat{W}\hat{u}^+$ is equivalent to the following convolution formula:

$$u^-(t) = \int_{-\infty}^{+\infty} W(t - \tau) u^+(\tau) d\tau \tag{7}$$

Actually, for each discrete frequency ω_j, there is a corresponding impedance $Z_j (j = 1, ..., N)$. Then we can define a softness coefficient:

$$\hat{\tilde{W}}_j(\omega) = \hat{W}_j(\omega) + 1 = \frac{2}{1 + Z_j} = \frac{2(1 + R_j - iX_j)}{(1 + R_j)^2 + X_j^2} \tag{8}$$

where R_j and X_j are the resistance and the reactance at the *jth* frequency and they are real. $\hat{\tilde{W}}_j(\omega)$ consists of a group of rational functions, which have known roots, as shown in the following expression:

$$\hat{\tilde{W}}_j(\omega) = \sum_{k=1}^{N} \frac{A_{2k-1} i\omega_j + A_{2k}}{(i\omega_j + \bar{\alpha}\omega_{0k})^2 + {\omega_{0k}}^2(1-\bar{\alpha}^2)} \tag{9}$$

where ω_{0k} is the inherent frequency, $\bar{\alpha} = 0.35$ is a smoothing factor. Then the time-domain impedance boundary condition can be expressed in a recursive formulation:

$$u^-(t) = -u^+(t) + \int_0^\infty \tilde{W}(\tau) u^+(t-\tau) d\tau \approx -u^+(t) + \sum_{k=1}^{N} \left[I_{2k-1}(t) + I_{2k}(t) \right] \tag{10}$$

where:

$$I_{2k-1}(t) = \mu_{2k-1} \frac{\Delta t}{2} \left[u^+(t) + e^{i\omega_{2k-1}\Delta t} u^+(t-\Delta t) \right] + e^{i\omega_{2k-1}\Delta t} I_{2k-1}(t-\Delta t) \tag{11}$$

$$I_{2k}(t) = \mu_{2k} \frac{\Delta t}{2} \left[u^+(t) + e^{i\omega_{2k}\Delta t} u^+(t-\Delta t) \right] + e^{i\omega_{2k}\Delta t} I_{2k}(t-\Delta t) \tag{12}$$

The coefficients μ_{2k-1}, μ_{2k}, ω_{2k-1}, ω_{2k} can be solved as Fung and Ju[15] proposed.

3.THE COMBINED SHAPE AND LINER OPTIMIZATION FRAMEWORK

3.1 GEK and Adjoint-based Shape Optimization Procedure

In this section, the GEK and adjoint-based shape design optimization is first performed. The shape optimization procedure is described in Fig.1.

1) the objective function is defined concerning the acoustic and the design variables are defined; based on that,the design space is specified by defining the independent variables and their range.

2) the Design-of-Experiment (DoE) theory, namely the Latin hypercube method,is used to generate a sets of sample points.

3) The aerodynamic aerodynamic flow-field at the samples points is calculated first, then the duct sound propagation is evaluated on the mean background flow.

4) The adjoint method is used to obtain all the gradient of design variables with high efficiency at the current design point.In the adjoint method, the sound propagation are calculated first by solving the MMLEE; then the adjoint equations based on MMLEE are solved; Next evaluates the gradients of the design variables.

5) The objective and the correlation matrix are both updated by including the solved gradient information from adjoint method. Based on that, the initial GEK model is constructed.

6) a search strategy is performed using the Gradient-enhanced Kriging model to identify new design points for aeroacoustic analysis.

7) Judge if the convergence is achieved or the stop conditions are satisfied.

8) Adding additional samples to those already available data base until the accuracy of the Gradient-enhanced Kriging model stops improving.

3.2 Kriging-based Liner Optimization Method

Based on the work of shape optimization, liner design problems are formulated based on the optimum inlet. The whole liner optimization algorithm in this approach is as follows, as also shown in Fig. 2.

1) In this study, the Latin hypercube method is used for the space-filling. A total of 50 sample points (liners) are selected from the initial search region.

2) The sample points are evaluated. The CAA computation of 50 sample liners were evaluated using a CAA code, respectively.

3) With the sample data obtained, the Kriging parameter is determined.

4) Once a Kriging model for objective values is constructed, the model should be validated. And predictions from the Kriging model are validated by comparing the results obtained by CAA calculations.

5) To obtain a more complete picture, a multi-Island genetic algorithm is used to obtain the Pareto front for the objective based on estimated objectives from the Kriging model.

6) Predictions from the pareto points are validated by comparing the results obtained by CAA results.

7) If the convergence is not achieved, add the newly available objective values to the data set and rebuild the Kriging model.

8) The whole process is repeated until some form of convergence is achieved, or an acceptable liner design has been obtained.

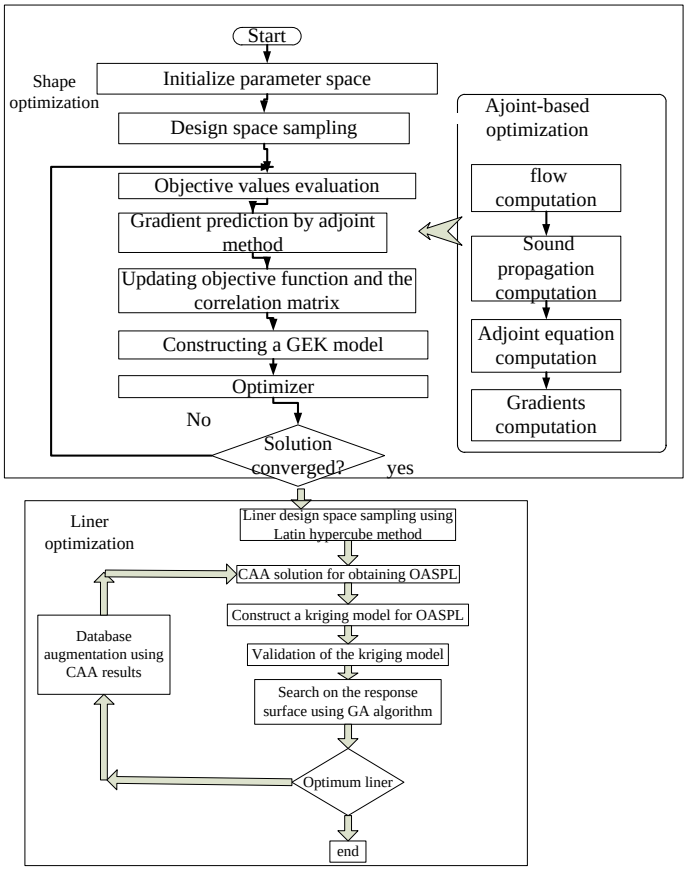

Fig. 1 the combined shape and liner optimization framework

4. NUMERICAL RESULTS

In this section, the proposed shape and liner optimization algorithm are applied to the design of a 2D inlet in an attempt to minimize the sound generation at the far-field.

The shape optimization for an axi-symmetric generic inlet case is carried out first. A buffer zone is used to absorb the reflective spurious waves, as well as to accommodate incoming modal waves inside the duct. Other buffer zones were placed around the outer boundaries of the computational domain. The background mean flows corresponding to take-off are solved by using ANSYS FLUENT 12.0. The desired convergent target of each CFD simulation is to make the root mean square residuals of the momentum and mass equations, energy equation, and turbulence equations reach or even lower than 1e-6.

The Hicks-Henne Shape Function[18] which are expressed as $b_i(x) = \sin^4\left(\pi x^{m_i}\right)$, $m_i = \ln(0.5)/\ln\left(x_{M_i}\right)$ is used to form the new duct geometry, where $b_i(x)$ are Hicks-Henne shape function. The inlet geometry can be parameterized by adding the baseline with the weighted sum of a number of sine "bump" functions. And the design variables are those shape functions. The 50 design variables distribute along the lower surface. Figs. 2 show the components of the gradients of the 50 design variables.

In order to validate the precision of the gradient values of 50 design variables, the gradient values obtained by using a finite-difference (FD) approach are compared again to those by the adjoint-based method. The figure 2 gives a good agreement on the comparison of the gradients by those two methods. This gradient accuracy is definitely good enough for an optimization procedure. Incorporate the gradients obtained from high efficient adjoint method, the GEKriging model constructs a accurate surrogate model.In this case, gradient norms, driven by the GEK model and the derivatives computed by the adjoint method, converged in 35 cycles in Fig. 3. The procedure searches further around the global optimum after achieving a minimum but finds no additional improvement. The convergence histories of the noise minimizations in Fig. 3 show that this objective function is mainly reduced in the first 20 iterations and that the gradient norm value are reduced significantly. The sum amplitude of the sound pressure for the optimized shape is reduced to 86.2% of the initial value of the original geometry I= 6.25e-7, which is used to scale the objective function values to ease comparisons. The final optimized intake duct shape is compared together with the baseline in Fig.4. As the simulation results show, the GEK has the ablity of searching a larger design space and a bigger shape changes is observed.

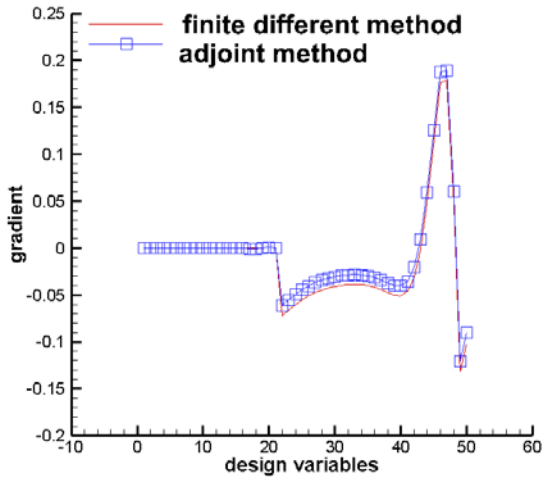

Fig. 2 Objective functional gradient components computed using the adjoint method and the finite-difference scheme.

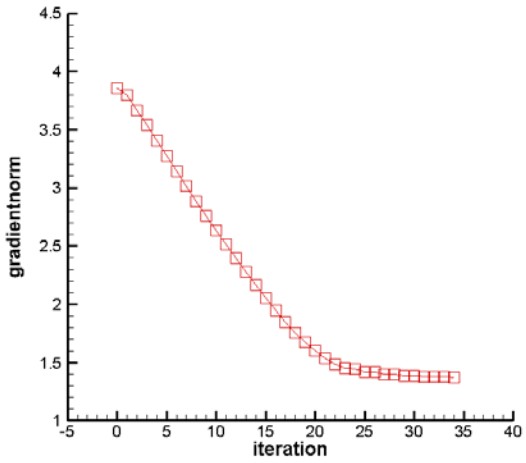

Fig. 3 convergence histories of the gradient norm

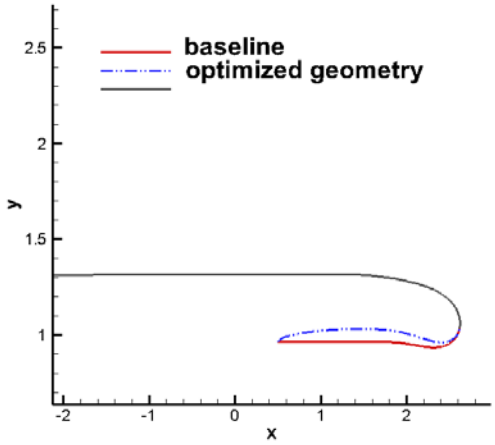

Fig.4 a comparison of the baseline and optimum intake duct geometry by using GEK and Kriging method

After the shape optimization using GEK and Kriging method, the liner optimization is then performed on this optimum intake duct geometry. The liner is modeled using the time domain impedance boundary condition described earlier. A cost function was defined by an averaging of all SPL differences at the grid points between x=1 units to x=2 units, namely $fun = \frac{1}{N}\sum_{i=1}^{N}\left(SPL_{liner} - SPL_{hardwall}\right)_i$,where M is the number of grid points. The liner optimization attempts to make the cost value as large as possible and obtain the optimum impedance values. There six discrete frequencies ranging from 0.5 kHz to 3.0 kHz with a sampling frequency interval of 0.5 kHz. The computational grid consists of 165000 cells and either the hard wall or the TDIBC was applied to the duct walls. The impedance data of a single cavity liner model[19] is used. An assumption of equal amplitude distribution was proposed and constant changes of the resistance R and the reactance X were also assumed at all discrete frequencies. And the resistance R and reactance X were given constant changes of ΔR and ΔX in each optimization operation.The optimized impedance values are listed in Table 1.

To evaluate the optimum inlet obtained by the shape optimization and liner optimization further, the sound propagation of near-field and the detail of flow-field are checked. Figure 8 shows pressure contours of hard wall case of baseline, which is

compared with the result of the optimized geometry with optimum liner. The acoustic pressure is solved for the (m,n)=(13,1) mode, the highest frequency of 3.0 kHz and comparisons of the predicted far field directivity between the baseline and the optimum geometry with liner are shown in Fig. 5, where far-field Sound Pressure Level(SPL) are on a 35 m circular arc, referenced to 20μPa. It can be seen from Fig. 6 that the overall directivity pattern in far-field is dominated about 60 degrees. It also shows that the liner optimization provides about a 2.3 dB reduction in the peak radiation angles, whereas the peak radiation angles differ from each other by about 1.3 deg. In other parts of the directivity, the patterns are also similar.

Table 1 Optimized impedance values

Frequency(KHz)	R	X
0.5	1.71	-1.50
1.0	0.66	0.26
1.5	1.22	1.61
2.0	4.25	0.88
2.5	1.75	-1.45
3.0	0.92	-0.16

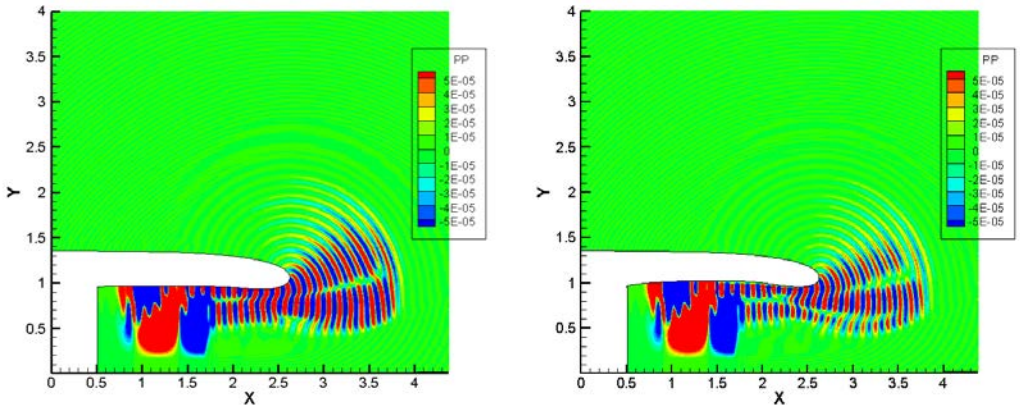

Fig. 5 (a) acoustic pressure contours of the baseline;(b) acoustic pressure contours of the optimized geometry and optimum liner.

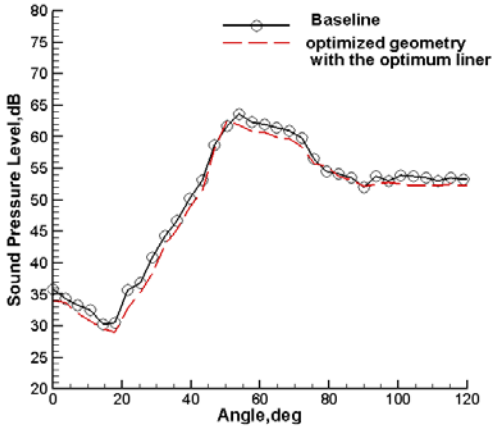

Fig. 6 Far-field directivity patterns of the baseline and the optimized geometry with optimized liner

5. CONCLUSIONS

This paper explores the use of a combined shape and liner optimization method to minimize the far-field sound from an inlet. Firstly, to obtain improved designs, a Gradient-enhanced Kriging (GEK) method in combination with a continuous adjoint methodology is applied in shape optimization method to design the inlet. An effective and efficiency method has been constructed after combining a Kriging response surface method with cheap gradient information using an adjoint method. The accuracy of the aeroacoustic adjoint method is validated by comparing the gradient values with those obtained by finite differences method. Secondly, after the shape optimization process, the acoustic liner on the lower duct wall is optimized based on the optimum intake geometry. The obtained results show that the combined shape and liner optimization can effectively change the sound pressure in near-field and directivity pattern in the far field, namely the optimum geometry with the optimized liner has a low noise performance. The results indicate that the combined optimization algorithm proposed, which uses a adjoint-based shape optimization approach in combination with a kriging-based liner optimization method, is effective and efficient used to optimize 2D inlet within a reasonable number of cycles to minimize the noise at a given far-field position. The next major step is the extension of the current method to three-dimensional problems.

6. ACKNOWLEDGEMENTS

This work is supported by National Natural Science Foundation of China (Grants 51506189) and Shanghai Engineering Research Center of Commercial Aircraft Engine.

7. REFERENCES

1. E. J.Rice, “Acoustic Liner Optimum Impedance for Spinning Modes with Mode Cutoff Ratio as Design Criterion”, AIAA Paper 76-516, pp. 1-13,(1976).
2. W. R. Watson, and J. H. Robinson, “*Design and Attenuation Properties of Periodic Checkerboard Liners”*, AIAA Paper 2003-3309,pp. 1-15,(2003).
3. R. E. Motsinger, R. E. Kraft, and J. W. Zwick, “*Design of optimum acoustic treatment for rectangular ducts with flow”*, American Society of Mechanical Engineers, no. 76-GT-113, 15-36,(1976)
4. J. A. Hamilton, and R. J. Astley, “*Theoretical Optimisation of an Intake Lip Liner for a A320/CFM56 Flight Tests*,Technical Report D1.2-3.5-11, Silencer Consortium, pp. 1-13,(2002).

5. L. Lafronza, A. McAlpine, A.J. Keane and R.J. Astley, *"Response surface method optimization of uniform and axially segmented duct acoustics liners"*,Journal of Aircraft, 43,1089-1102, (2006).
6. S. Zheng, M. Zhuang, and F.Thiele, *"Noise prediction and optimization system for turbofan engine inlet duct design"*, In: 10th AIAA/CEAS Aeroacoustics Conference, Manchester, AIAA 2004-3031, pp.1-10, (2004).
7. S. Shahpar, *"SOFT: A New Design and Optimisation Tool for Turbomachinery"*, Evolutionary Methods for Design, Optimisation and Control, CIMNE, Barcelona, pp.1-12, (2002)
8. F. L Pan, and J. Coupland, *"An Integrated Optimization System for Low Noise Nacelle Design"*, In: 11th AIAA/CEAS Aeroacoustics Conference (26th AIAA Aeroacoustics Conference), Monterey, California, AIAA 2005-2945, pp.1-16,(2005).
9. R. Sugimoto, and R. J. Astley, *"Validation and application of a hybrid prediction scheme for bypass duct noise"*, In: 12th AIAA/CEAS Aeroacoustics Conference, Cambridge, MA, USA, AIAA paper 2006-2520,pp.1-13, (2006).
10. C. McAleer , R. J. Astley, , K. Holland, , R. Sugimoto, , and A. Kempton, *" Fan Noise Propagation within Curved Bypass Ducts with 3D Features"*, In: 14th AIAA/CEAS Aeroacoustics Conference (29th AIAA Aeroacoustics Conference), Vancouver, British Columbia Canada, AIAA 2008-2878, pp.1-16, (2008)
11. W. Liu, "*Development of Gradient-enhanced Kriging approximations for multidisciplinary design optimisation*", Ph.D. dissertation, University ofNotre Dame, Notre Dame, Indiana, (2003).
12. A. Jameson, "*Optimum aerodynamic design using CFD and control theory*", AIAA Paper 95-1729-CP, (1995).
13. J.E. Ffowcs Williams, D.L. Hawkings, *"Sound generated by turbulence and surfaces in arbitrary motion"*, Philos Trans Royal Soc Lond, 1969, A264,321–42, (1969).
14. Zhang, X., and Chen, X.X. *"Time-Domain Computation of Multimode Propagation in an Aero-engine Duct"*, Procedia Engineering 6,173–182, (2010)
15. Selvakumar Ulaganathan, Ivo Couckuyt, and Joris Degroote. *"ON THE USE OF GRADIENTS IN KRIGING SURROGATE MODELS"*, Proceedings of the 2014 Winter Simulation Conference,(2014).
16. Qiu, S. *"A continuous adjoint-based aeroacoustic shape optimization for multi-mode duct acoustics"*, Proc IMechE Part C: J Mechanical Engineering Science 20(3) 1–18, (2017).
17. Ju, H. B., and Fung, K. Y., *"Time-Domain Impedance Boundary Conditions with Mean Flow Effects"*,AIAA Journal, 39 (9), pp. 1683-1690, (2001).
18. Hicks, R. M., and Henne, P. A. *"Wing design by numerical optimization"*, Journal of Aircraft, 15, 407–412, (1978).
19. Motsinger, R. E. and Kraft, R. E., *"Design and Performance of Duct Acoustic Treatment,"* Aeroacoustics of Flight Vehicles: Theory and practice, 2: Noise Control, pp. 165-205, (1991).